Diseases of the nervous system associated with calcium channelopathies

Todorov, B.B.

HIGH CORTICAL SPREADING DEPRESSION SUSCEPTIBILITY AND MIGRAINE-ASSOCIATED SYMPTOMS IN $CA_V2.1$ S218L MICE

Arn M. J. M. van den Maagdenberg[1,2*], Tommaso Pizzorusso[3*], Simon Kaja[2,3,$,*], Nicole Terpolilli[6*], Maryna Shapovalova[7], Freek E. Hoebeek[8], Curtis F. Barrett[1,2], Lisa Gherardini[5], Rob C.G. van de Ven[1], Boyan Todorov[1], Ludo A.M. Broos[1], Angelita Tottene[7], Zhenyu Gao[8], Mariann Fodor[4†], Chris I. De Zeeuw[8,9], Rune R. Frants[1], Nikolaus Plesnila[6], Jaap J. Plomp[2,3], Daniela Pietrobon[7] and Michel D. Ferrari[2]

Departments of [1]Human Genetics, [2]Neurology, [3]Molecular Cell Biology–Section Neurophysiology, and [4]Embryology & Anatomy, Leiden University Medical Centre, Leiden, The Netherlands; [5]Department of Psychology, University of Firenze and CNR Institute of Neuroscience, Pisa, Italy; [6]Department of Neurosurgery and Institute for Surgical Research, University of Munich Medical Centre – Grosshadern, Munich, Germany; [7]Department of Biomedical Sciences, University of Padova and CNR Institute of Neuroscience, Padova, Italy; [8]Department of Neuroscience, Erasmus Medical Centre, Rotterdam, The Netherlands; [9]Netherlands Institute for Neuroscience, Royal Dutch Academy for Sciences (KNAW), Amsterdam, The Netherlands;

*Authors contributed equally; [$]Present address: Department of Ophthalmology University of Missouri Kansas City, School of Medicine, Kansas City, USA; †Dr Mariann Fodor is deceased.

Ann Neurol. 2010;67:85-98

ABSTRACT

Objective: The *CACNA1A* gene encodes the pore-forming subunit of neuronal $Ca_V2.1$ channels. In patients, the S218L *CACNA1A* mutation gives rise to a dramatic hemiplegic migraine syndrome that is associated with ataxia, seizures, and severe, sometimes fatal, brain edema often triggered by only a mild head trauma.

Methods: We introduced the S218L mutation into the mouse *Cacna1a* gene and studied the mechanisms for the S218L syndrome by analyzing the phenotypic, molecular, and electrophysiological consequences.

Results: *Cacna1a*^{S218L} mice faithfully mimic the associated clinical features of the human S218L syndrome. S218L neurons exhibit a gene dosage-dependent negative shift in voltage dependence of $Ca_V2.1$ channel activation, resulting in enhanced neurotransmitter release at the neuromuscular junction. *Cacna1a*^{S218L} mice also display an exquisite sensitivity to cortical spreading depression (CSD), with a vastly reduced triggering threshold, an increased propagation velocity, and frequently multiple CSD events after a single stimulus. In contrast, mice bearing the R192Q *CACNA1A* mutation, which in humans causes a milder form of hemiplegic migraine, typically exhibit only a single CSD event after one triggering stimulus.

Interpretation: The particularly low CSD threshold and the strong tendency to respond with multiple CSD events make the S218L cortex highly vulnerable to weak stimuli and may provide a mechanistic basis for the dramatic phenotype seen in S218L mice and patients. Thus, the S218L mouse model may prove a valuable tool to further elucidate mechanisms underlying migraine, seizures, ataxia, and trauma-triggered cerebral edema.

Keywords: Calcium channel, mild head impact, seizure, hemiplegic migraine, synaptic transmission, transgenic

INTRODUCTION

Familial Hemiplegic Migraine (FHM) is an autosomal dominant subtype of migraine in which attacks are associated with transient hemiparesis and other neurological aura symptoms (*International Headache Society, 2004*). We consider FHM a valid monogenic model for studying pathogenetic mechanisms that are involved in the genetically more complex common forms of migraine. The arguments for this are mainly clinical and include: (1) the headache and aura features of FHM and common migraine attacks are, apart from the hemiparesis, identical; (2) two-thirds of FHM patients have, in addition to attacks of FHM, attacks of common non-hemiplegic migraine; (3) two-thirds of their first-degree relatives have attacks of common non-hemiplegic migraine; (4) both FHM and common migraine attacks can be precipitated by similar trigger factors and can be prevented with the same prophylactic agents; and (5) their headache phases can be aborted with the same acute treatments (*Ferrari et al., 1998*; *Terwindt et al., 1998*; *Ducros et al., 2001*; *Ferrari & Goadsby, 2006*).

FHM has been linked to three genes, all of which encode proteins that drive or regulate neuronal excitability (for review, see *van den Maagdenberg et al., 2007*; *Pietrobon, 2007*). FHM1 is caused by mutations in the *CACNA1A* gene (*Ophoff et al., 1996*; *van den Maagdenberg et al., 2007*; *Pietrobon, 2007*; *Adams & Snutch, 2007*; *Stam et al., 2008*) that encodes the α_{1A}-subunit of neuronal $Ca_V2.1$ (P/Q-type) voltage-gated calcium channels, which couple presynaptic Ca^{2+} entry to synaptic neurotransmitter release (*Catterall, 1998*). Functional studies in heterologous expression systems support a net gain-of-function effect of FHM1 mutations (*Hans et al., 1999*; *Tottene et al., 2002*; *Tottene et al., 2005*; but also see *Kraus et al., 1998*; *Kraus et al., 2000*; *Cao et al., 2004*; *Cao & Tsien, 2005*; *Barrett et al., 2005*). In an analysis of the single-channel properties of eight different FHM1 mutations, open probability (and therefore integrated Ca^{2+} current) was increased over a broad voltage range, resulting in a shift to lower voltages for channel activation (*Hans et al., 1999*; *Tottene et al., 2002*; *Tottene et al., 2005*). Consistent with these findings, cerebellar granule and cortical pyramidal neurons from knockin mice carrying the FHM1 R192Q mutation exhibited significantly increased P/Q-type current density at negative voltages (*van den Maagdenberg et al., 2004*; *Tottene et al., 2009*). These mice also showed enhanced excitatory transmission at cortical synapses due to increased action-potential evoked Ca^{2+} influx and increased probability of glutamate release (*Tottene et al., 2009*) and, as a consequence, a decreased triggering threshold for cortical spreading depression (CSD) (*van den Maagdenberg et al., 2004*; *Tottene et al., 2009*). CSD is a slowly propagating wave of cortical neuronal and glial depolarization that underlies the migraine aura (*Lauritzen, 1994*) and may possibly activate migraine headache mechanisms (*Bolay et al., 2004*).

While the *CACNA1A*^{R192Q}, and most other FHM1 mutations, give rise to only mild forms of FHM1, which are not associated with additional major neurological features (*Ophoff et al., 1996*; *Pietrobon, 2007*; *Haan et al., 2005*), the *CACNA1A*^{S218L} FHM1 mutation may cause a particularly dramatic clinical syndrome. This "S218L syndrome" may consist

of, in addition to attacks of hemiplegic migraine, slowly progressive cerebellar ataxia, epileptic seizures, and severe, sometimes fatal, cerebral edema which can already be triggered by only a trivial head trauma (*Fitzsimons & Wolfenden, 1985*; *Kors et al., 2001*; *Curtain et al., 2006*; *Chan et al., 2008*).

In order to understand how a single amino acid substitution can account for such a wide range of neurological features, we generated transgenic knockin mice bearing the S218L missense mutation in the *Cacna1a* gene, and examined the clinical and functional consequences of the mutation. This provided a unique opportunity to study shared pathogenetic mechanisms, not only of FHM and common migraine, but also of cerebellar ataxia, epilepsy, and mild head trauma-triggered cerebral edema, each of which has also been linked with common types of migraine (*Blau & Solomon, 1985*; *Meaney et al., 1996*; *Sándor et al., 2001*; *Cha et al., 2007*; *Ambrosini et al., 2008*; *Rogawski, 2008*; *Haan et al., 2008*).

We found that *Cacna1a*^{S218L} mice indeed display the main associated clinical features of the human "S218L syndrome". In addition, these mice exhibit a number of important neurobiological changes. These include: (1) highly increased neuronal Ca^{2+} influx through $Ca_V2.1$ channels; (2) strongly increased spontaneous release of neurotransmitter at the neuromuscular junction; and (3) a dramatically reduced triggering threshold for CSD, with an increased propagation velocity and an increased probability of multiple CSD events upon a single stimulation. We believe that the unique vulnerability to CSD may explain many of the dramatic features of the S218L syndrome. Moreover, the *Cacna1a*^{S218L} mouse may prove a valuable tool to study shared pathogenetic mechanisms of brain disorders that may model or are frequently co-occurring with common types of migraine.

EXPERIMENTAL PROCEDURES

Generation of transgenic *Cacna1a*^{S218L} mice

The generation of *Cacna1a*^{R192Q} mice was previously described (*van den Maagdenberg et al., 2004*). To generate *Cacna1a*^{S218L} mice, the *Cacna1a* gene was modified using a gene-targeting approach so that exon 5 contained the human FHM1 S218L mutation. In the targeting vector the original TCA triplet codon 218 was changed into TTA by site-directed mutagenesis, creating the S218L mutation. Upstream of exon 5, a PGK-driven neomycin cassette flanked by LoxP sites was introduced. Embryonic stem cells (E14) were electroporated and positive clones were screened for homologous recombination by Southern blot analysis using the external probes indicated in *Figure 1A*. The presence of the S218L mutation was confirmed by PCR amplification of exon 5 using primers 271 (5'-CTCCATGGGAGGCACTTG-3') and 272 (5'-ACCTGTCCCCTCTTCAAAGC-3') and subsequent digestion with restriction enzyme *VspI* as well as direct sequencing of the PCR products. Correctly targeted ES cells were injected into C57Bl/6J blastocysts

to create chimaeric animals. Offspring that were heterozygous for the S218L+Neo allele were crossed with EIIA-*Cre* deleter mice (*Lakso et al., 1996*) to excise the neomycin cassette. *Cacna1a*^{S218L} mice in which the neomycin cassette was successfully deleted were backcrossed to C57Bl/6Jico mice. *Cacna1a*$^{S218L/WT}$, *Cacna1a*$^{S218L/S218L}$, and wild-type littermates of the third generation were used for all analyses (~87.5% C57Bl/6Jico and ~12.5% 129Ola background). Genotyping of mice for all experiments was performed by PCR analysis as described above. All animal experiments were performed in accordance with the guidelines of the respective institutions and national legislation. The studies were performed using a similar number of male and female mice and summary data show results from both genders. For all experiments, the investigator was blinded to the genotype.

RNA analysis

For RNA extraction, mice were killed by cervical dislocation and forebrain and cerebellum were dissected in 0.1 M ice-cold phosphate-buffered saline (pH 7.4) and subsequently snap-frozen in liquid nitrogen. For Northern blot and RT-PCR experiments, RNA was isolated as previously described described (*van den Maagdenberg et al., 2004*). For Northern blot analysis, 10 μg of cerebellar RNA was separated on a 1% agarose gel and subsequently transferred to a Hybond-N+ membrane (*Amersham Biosciences, Buckinghamshire, UK*). ^{32}P-labeled PCR products of *Cacna1a* or *Cyclophilin* cDNA were used as probes using standard hybridization and washing conditions.

Rotarod

The accelerating Rotarod (*UGO Basile S.R.L., Commerio VA, Italy*) test was performed on a 4-cm diameter horizontal rotating rod. The test was performed in a semi-dark room with a light source placed at the bottom to discourage the mice from jumping off the Rotarod. Mice (8-10 weeks of age) were tested in groups of five. Following a training period (in which the mice were placed on the Rotarod turning at a low constant speed of 5 rpm for 5 min), the mice were subjected to six consecutive days of trials (one trial per day). Each trial started with the Rotarod turning at a constant speed of 5 rpm for 10 s, after which the speed was gradually increased to 45 rpm over the following 5 min. The latency to fall (i.e., endurance) was recorded, and the endurance per trial per genotype is presented as mean ± SEM.

Electroencephalography

EEG electrodes were surgically implanted under isoflurane anesthesia in 10-14-weeks old mice. Six 1-mm diameter stainless steel screw electrodes were positioned as follows: one in each frontal bone and one in each medial bone for recording activity patterns from primary motor and parietal cortices, respectively. The remaining two electrodes (placed in the temporal bone) served as reference (medial) and ground (lateral) electrodes. Isolated copper wire was used to attach the electrodes to a mini-connector that was cemented

to the skull with dental acrylic. Recording began 2hrs after surgery. For recording, animals were placed in an electrically-shielded sound-proof box for continuous EEG recording and simultaneous video observation. Electrical signals were amplified, filtered (*CyberAmp, Molecular Devices, Sunnyvale, CA*), digitized (*1401Plus, Cambridge Electronic Design, Cambridge, UK*), and stored for off-line analysis (*Spike2, Cambridge Electronic Design*). Differential EEG signals were sampled at 500 Hz and filtered using a bandpass of 0.1-30 Hz.. The behavior of the mice was continuously monitored with a video camera and recorded at 25 frames per second using custom-made software (*Labview, National Instruments, Austin, TX*). Recording lasted up to 48 h, during which food and water were available *ad libitum*.

Survival analysis

Survival curves were constructed using the method of Kaplan and Meier (*Kaplan & Meier, 1958*). The survival curves were compared by the log rank test. Survival times were calculated from the date of birth to the date of death. Mice that died of unknown cause (that is, not related to an experimental intervention) were considered cases. Statistical analysis was performed using SPSS 10.0 software (*SPSS Inc., Chicago, IL*).

In vivo model of cerebral impact and quantification of brain edema

Anesthesia was initiated in an isofluorane chamber (4%) and was maintained thereafter with 1.5% isofluorane in 30% oxygen/68.5% nitrous oxide supplied by a face mask. Mild impact was induced essentially as previously described (*Chen et al., 1996*), but with the important difference that the *intensity* of the weight drop was considerably diminished by reducing the height from where the weight was dropped from 72 to 15 cm. Whereas a weight drop from 72 cm causes severe neurological deficits and high mortality (> 30%) in wild-type mice, the modified low-height mild-impact protocol did not cause neither mortality nor any obvious neurological dysfunction in wild-type mice. Briefly, the animal's head was fixed in a stereotactic frame and the skull was exposed by a midline incision. Body temperature was kept constant at 37°C using a feedback-controlled heating pad connected to a rectal probe (*Heater Control Module, FHC, Bowdoinham, ME*). Impact to the brain was applied by dropping a 72 g weight guided through a plastic tube onto the skull from a height of 15 cm. Immediately after the impact, the skin was closed and animals were transferred to an incubator heated to 35°C until recovery of spontaneous motor activity (30 min). Brain water content was determined as previously described (*Vakili et al., 2005*; *Zweckberger et al., 2006*). Briefly, 24 h after impact, the mice were sacrificed and their brains were removed. After removal of the pons and olfactory bulb, the brains were weighed in order to obtain their wet weight (ww), dried at 110°C for 24 h, and then re-weighed to obtain their dry weight (dw). Brain water content (expressed as percentage) was calculated using the formula ((ww – dw) / ww) × 100.

$Ca_V2.1$ current in cerebellar granule cells

Cerebellar granule cells were grown in primary culture from 6-day-old mice as previously described (*Fletcher et al., 2001*). Experiments were performed on cells grown from 6 to 7 days *in vitro*. Whole-cell patch-clamp recordings were performed at room temperature as described previously (*Fletcher et al., 2001*; *Tottene et al., 2009*). The external recording solution contained (in mM): $BaCl_2$ 5, tetraethylammonium (TEA)–Cl 148, Hepes 10, and 0.1 mg/ml cytochrome C, pH 7.4 with TEA-OH. The internal solution contained (in mM): Cs-methanesulfonate 100, $MgCl_2$ 5, Hepes 30, EGTA 10, ATP 4, GTP 0.5, and cAMP 1, pH 7.4 with CsOH. Currents were low-pass filtered at 1 kHz and digitized at 5 kHz. Compensation (typically 70%) for series resistance was generally used. Current-voltage (*I-V*) relationships were obtained only from cells with a voltage error of <5 mV and without signs of inadequate space clamping such as notch-like current discontinuities, slow components in the decay of capacitive currents (in response to hyperpolarizing pulses) or slow tails not fully inhibited by nimodipine. The average normalized *I-V* curves were multiplied by the average maximal current density obtained from all cells. *I-V* curves were fitted with the equation: $I_{Ba} = G\times(V–E_{rev})/(1+e\text{^}((V_{0.5}–V)/k))$ using a non-linear regression method based on the Levenberg-Marquardt algorithm. The liquid junction potentials were such that a value of 12 mV should be subtracted from all voltages to obtain the correct values of membrane potential in whole-cell recordings (*Fletcher et al., 2001*). All drugs were stored as stock solutions at –20°C: 250 μM ω-conotoxin-GVIA (ω-CgTx-GVIA; *Bachem, Budendorf, Switzerland*) and 250 μM ω-conotoxin-MVIIC (ω-CTx-MVIIC; *Bachem, Budendorf*) in distilled water, and 10 mM nimodipine (*a gift from Dr. Hof, Sandoz, Basel, Switzerland*) in 95% ethanol.

Ex vivo neuromuscular junction electrophysiology

The neuromuscular junction (NMJ) is a model synapse in the peripheral nervous system, that exclusively relies on presynaptic $Ca_V2.1$ channels (*Uchitel et al., 1999*) and can be electrophysiologically analyzed with relative ease to investigate neurotransmission. Mice (~2 months of age) were euthanized by carbon dioxide inhalation. Phrenic nerve–hemidiaphragms were dissected and mounted at room temperature in standard Ringer's medium containing (in mM): NaCl 116, KCl 4.5, $CaCl_2$ 2, $MgSO_4$ 1, NaH_2PO_4 1, $NaHCO_3$ 23, and glucose 11, pH 7.4. The solution was continuously bubbled with 95% O_2 / 5% CO_2.

Intracellular recordings of miniature endplate potentials (MEPPs) (the small spontaneous depolarizing events due to uniquantal acetylcholine [ACh] release) and endplate potentials (EPPs) (the depolarization resulting from nerve action potential–evoked ACh release) were performed at NMJs at 28°C using standard micro-electrode equipment as previously described (*Kaja et al., 2005*; *Kaja et al., 2007*). At least 30 MEPPs and EPPs were recorded at each NMJ, and typically 7-15 NMJs were sampled per experimental condition per muscle. Muscle action potentials were prevented with

the muscle-specific sodium channel blocker μ-conotoxin-GIIIB (3 μM; *Scientific Marketing Associates, Barnet, Herts, UK*). EPPs were recorded in Ringer´s medium as above, except also containing 0.2 mM Ca^{2+}. The nerve was electrically stimulated with 100-μs supramaximal pulses delivered at 0.3 Hz. Amplitudes of EPPs and MEPPs were normalized to –75 mV, assuming 0 mV as the reversal potential for ACh-induced current (*Magleby & Stevens, 1972*). The normalized EPP amplitudes were corrected for non-linear summation (*McLachlan & Martin, 1981*) with an *f* value of 0.8. The quantal content at each NMJ (i.e., the number of ACh quanta released per nerve impulse) was calculated by dividing the normalized, corrected mean EPP amplitude by the normalized mean MEPP amplitude.

Cortical spreading depression

For cortical spreading depression (CSD) experiments, *Cacna1a*^{S218L}, and for comparison *Cacna1a*^{R192Q}, transgenic, and wild-type mice (20-30 g) were anaesthetized with urethane (20% in saline; 6 ml/kg i.p.). The mice were mounted in a stereotaxic apparatus and continuously monitored for adequate level of anesthesia, temperature, heart rate, and lack of nociceptive reflexes. To record CSD, three holes were drilled in the skull over the left hemisphere. The first corresponded to the occipital cortex and was used for access of the electrical stimulation electrode. The second hole, at the parietal cortex (1 mm lateral and 1 mm caudal to Bregma), and the third hole, at the frontal cortex (1 mm lateral and 1 mm rostral to Bregma), were used for placement of the recording electrodes. The dura was carefully removed from a small part of the cortex using a 28-gauge needle, sufficient to let the recording electrode (tip diameter of 3 microns) enter the cortex. The steady-state (DC) potential was recorded with glass micropipettes placed 200 μm below the dural surface. An Ag/AgCl reference electrode was placed subcutaneously above the nose. Cortical stimulation was conducted using a copper bipolar electrode placed on the cortex after removing the dura. Pulses of increasing intensity (from 10 up to 800 μA) were applied for 100 ms at 3-min intervals with a stimulus isolator/constant current unit (*WPI Inc., Sarasota, FL*) until a CSD event was observed. The minimal stimulus intensity at which a CSD event was elicited was taken as the CSD threshold. Once a CSD event was elicited, the recording continued for 1h without stimulation, and additional CSD events were noted. The percentage of mice with multiple CSD events was determined only from those mice that could be recorded for one full hour following the first detected event. In some wild-type mice, the CSD induction threshold was re-assessed at the end of the one-hour monitoring of recurrent CSDs and found to be unchanged from the initial threshold, suggesting that general recording conditions remain stable for at least one hour. To measure CSD propagation velocity, the distance between the two recording electrodes was divided by the time elapsed between the CSD onset at the first and the second recording sites. The condition of the cortex was monitored using a surgical microscope and animals with lesions were excluded.

Statistical analysis

Statistical differences were analyzed with paired or unpaired Student's *t*-test, analysis of variance (ANOVA) with Tukey's HSD post-hoc test, Fisher's exact test, repeated-measures ANOVA, or Kruskal-Wallis one-way ANOVA on ranks followed by Dunn's Comparison Procedure as post-hoc test, all where appropriate. Calculations were performed with a statistical software package (*SigmaStat 3.0, Erkrath, Germany*). For all experiments, summary data are presented as mean ± SEM, and $p<0.05$ was considered to be statistically significant.

RESULTS

Generation of the S218L knockin mice

Using a gene-targeting approach with homologous recombination, we introduced the human *CACNA1A*^{S218L} mutation into the orthologous *Cacna1a* gene (*Fig. 1A, B*) to generate *Cacna1a*^{S218L} mice. RNA (*Fig. 1C*) and protein analyses (*Supplementary Fig.1*)

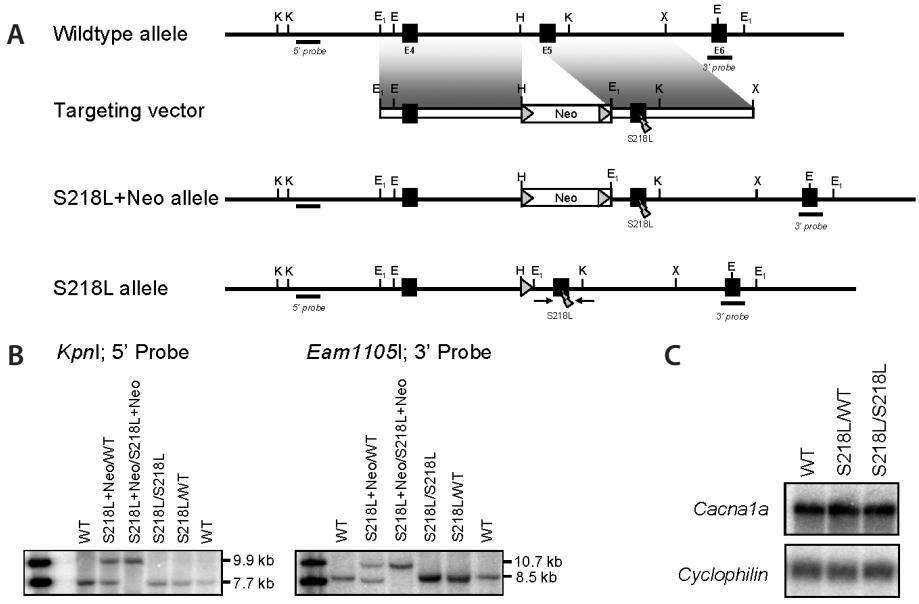

Figure 1. Generation of *Cacna1a*^{S218L} knockin mice. (A) Genomic structure of the wild-type *Cacna1a* allele, the targeting vector, and the predicted structure after homologous recombination (S218L+Neo allele), and following Cre-mediated deletion of the neomycin cassette (S218L allele). LoxP sites are indicated by triangles. Black numbered boxes indicate respective exons, with the S218L mutation in E5. Thick black lines indicate probes for Southern blot analysis. Primers used for genotyping and confirmation of the S218L mutation are depicted schematically with arrows. Restriction sites: E, *Eam1105*I; E_1, *Eco*RI; H, *Hind*III, K, *Kpn*I; X, *Xba*I. **(B)** Southern blot for all genotypes of S218L+Neo and S218L allele carriers showing genomic DNA digested with *Kpn*I or *Eam1105*I and tested with the 5'- or 3'-probe, respectively. **(C)** Northern blot of adult wild-type, *Cacna1a*$^{S218L/WT}$, and *Cacna1a*$^{S218L/S218L}$ brains. Total brain RNA was hybridized with *Cacna1a* and *Cyclophilin* cDNA probes. Note that *Cacna1a* message levels are similar among genotypes.

indicated that neither the mutation nor the introduction of the LoxP site seemed to have interfered with any major regulatory sequence as no major effect on *Cacna1a* expression with respect to quantity or location was observed. However, the experiments were not designed to reveal minor differences in *Cacna1a* expression.

S218L mice exhibit main features of the human S218L syndrome

Cacna1a$^{S218L/S218L}$ mice showed a complex neurological phenotype that is remarkably similar to that seen in *CACNA1A*^{S218L} patients (*Fig. 2A*). Most of the time, the mice appeared phenotypically normal, except for mild cerebellar ataxia. The ataxia was reflected by poor performance in the Rotarod test (*Fig. 2B*), accompanied by reduced arborization solely of proximal, primary dendrites of cerebellar Purkinje neurons (*Fig. 2C and Supplementary Fig. 2A*). These primary dendrites in *Cacna1a*$^{S18L/S218L}$ had a decreased length (*Supplementary Fig. 2B*). Purkinje cells of 2 months old S218L mice showed abnormal distal turns and a "weeping willow" appearance (*Fig. 2C*) similar to what has been reported for aged (> 1 year) *rocker* mice, which carry the naturally occurring *Cacna1a*^{T1310K} missense mutation (*Zwingman et al., 2007*).

We observed two types of spontaneous attacks in *Cacna1a*$^{S218L/S218L}$ mice: (1) attacks of hemiparesis, which are consistent with the attacks of hemiparesis seen in S218L FHM1 patients; and (2) attacks of generalized seizures that were in some cases fatal. The hemiparetic attacks consisted of brief periods of apparent transient unilateral weakness, manifesting as slow circular locomotion (due to leg movement only on one side of the body) and attempts to support themselves against the cage wall on the side of the hemiparesis. Following such episodes, the mouse would remain immobile for about 20 min and then recover. Some of these attacks were captured on video (see *Supplementary movie* for an example). In addition to the hemiparetic attacks, we also observed attacks which started with myoclonic jerks and subsequently evolved into generalized tonic-clonic ("grand mal") seizures. We were able to capture and analyze several of such episodes in three mice with an EEG recording coupled to video monitoring (*Fig. 2D*; see also *Supplementary note 1*). All three mice died at the end of such an episode.

In line with the observation that mice can die after spontaneous epileptic attacks, the life expectancy of mice, kept in their home cage environment (without experimental interventions), was significantly decreased (*Fig. 2E*). Post-mortem analysis indicated (data not shown) that the likely cause of death was lung edema, a frequent finding in epilepsy-related deaths, often secondary to cardiac arrest. Pathological examination excluded myocardial infarction, or other morphological abnormalities, in these cases. Additional histology of homozygous S218L brain material at the light microscope level did not reveal obvious structural abnormalities such as neurodegeneration (*data not shown*). The above-described spontaneous episodes of hemiparesis, the fatal seizures, and the reduced life expectancy, all appear to be unique to *Cacna1a*$^{S218L/S218L}$ mice; none were observed in *Cacna1a*$^{S218L/WT}$ (*Fig. 2*), nor in mice carrying the R192Q mutation

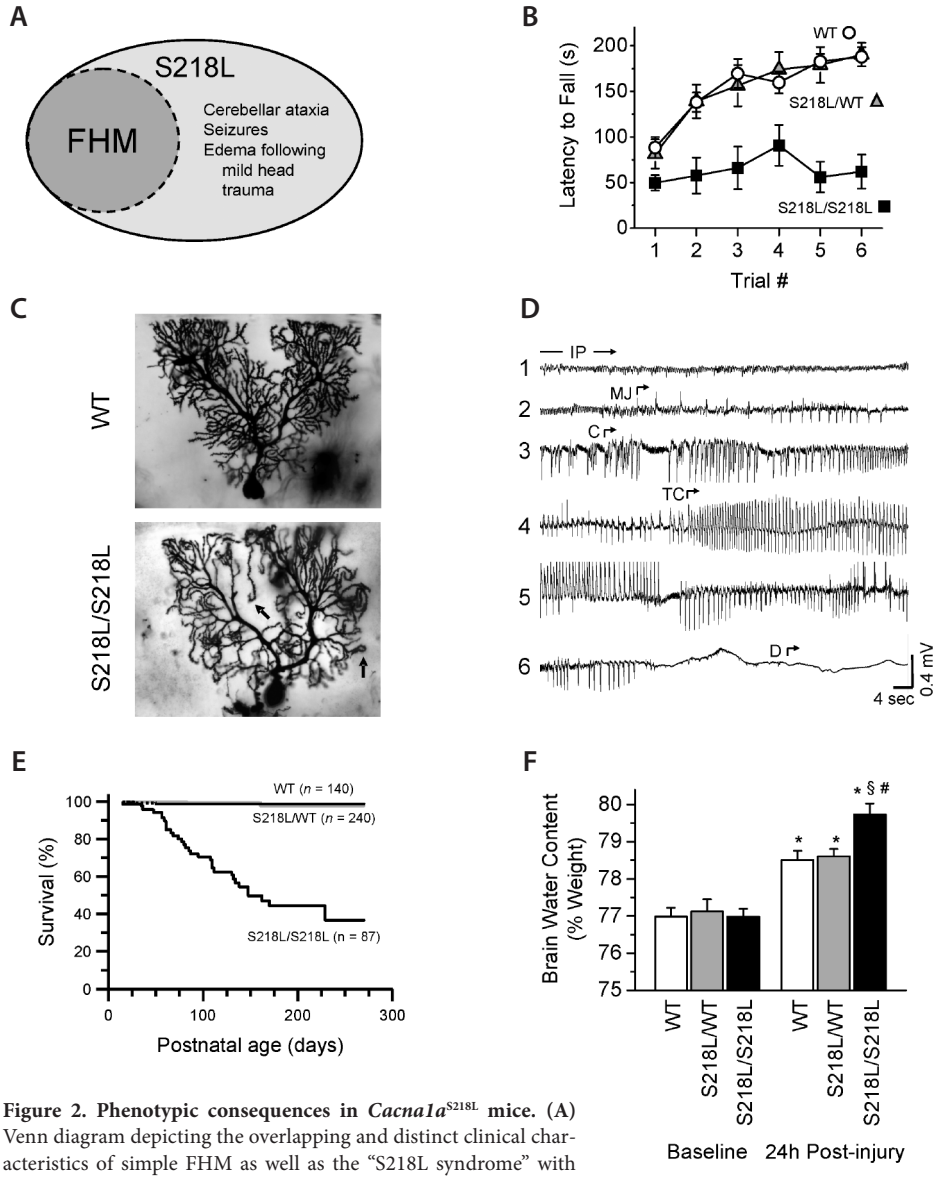

Figure 2. Phenotypic consequences in *Cacna1a*^{S218L} mice. (A) Venn diagram depicting the overlapping and distinct clinical characteristics of simple FHM as well as the "S218L syndrome" with severe associated features exhibited in S218L patients. **(B)** Rotarod testing for ataxia in 2-month-old mice reveals severe impairments in both performance and learning for *Cacna1a*$^{S218L/S218L}$ (n = 10-11). Trials were performed on consecutive days. **(C)** Golgi-Cox staining of cerebellar Purkinje neurons from 2-month-old wild-type and *Cacna1a*$^{S218L/S218L}$ mice. Arrows indicate decreased branching and downturned ends in the *Cacna1a*$^{S218L/S218L}$ neuron. **(D)** Long-term EEG recording of a *Cacna-1a*$^{S218L/S218L}$ mouse showing sequential phases (1-6) of a "grand mal" fatal seizure. Concurrent video monitoring was used to assess the overt clinical phenotype, described as follows: IP, interictal period; MJ, myoclonic jerks; C, clonic seizure, TC, tonic-clonic seizure; D, death. **(E)** Kaplan-Meier plot showing significantly decreased survival of *Cacna1a*$^{S218L/S218L}$ mice ($p < 0.001$ vs. WT). **(F)** Twenty-four hours after mild head impact (see Material and Methods), *Cacna1a*$^{S218L/S218L}$ mice had increased cerebral water content (n = 9, 15, and 5 mice for WT, *Cacna1a*$^{S218L/WT}$, and *Cacna1a*$^{S218L/S218L}$, respectively; *, $p<0.05$ vs. WT; #, $p<0.05$ vs. S218L/WT).

(*Cacna1a*$^{R192Q/R192Q}$), which in patients is associated with a much milder form of hemiplegic migraine (*Pietrobon, 2007*).

Consistent with observations in S218L patients, *Cacna1a*$^{S218L/S218L}$ mice, but not wild-type or *Cacna1a*$^{S218L/WT}$ mice, exhibited significant brain edema 24 hours after mild head impact as applied in our modified low-height weight-drop model (*Fig 2F*). The

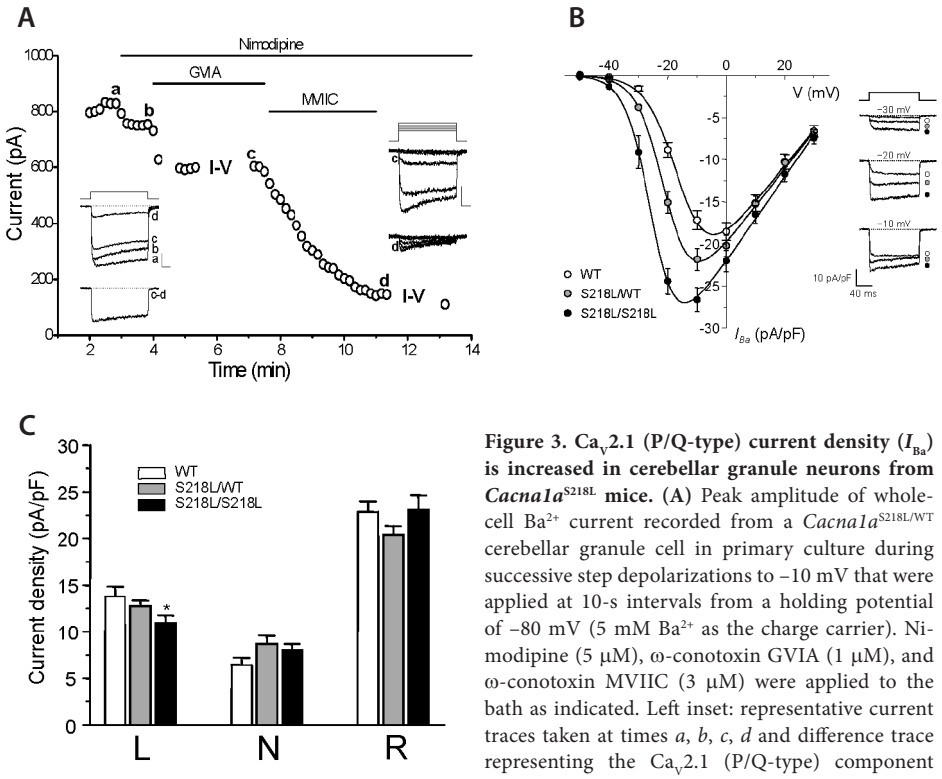

Figure 3. $Ca_V2.1$ (P/Q-type) current density (I_{Ba}) is increased in cerebellar granule neurons from *Cacna1a*^{S218L} mice. (A) Peak amplitude of whole-cell Ba^{2+} current recorded from a *Cacna1a*$^{S218L/WT}$ cerebellar granule cell in primary culture during successive step depolarizations to –10 mV that were applied at 10-s intervals from a holding potential of –80 mV (5 mM Ba^{2+} as the charge carrier). Nimodipine (5 μM), ω-conotoxin GVIA (1 μM), and ω-conotoxin MVIIC (3 μM) were applied to the bath as indicated. Left inset: representative current traces taken at times *a*, *b*, *c*, *d* and difference trace representing the $Ca_V2.1$ (P/Q-type) component (*c*-*d*). Right inset: representative traces at increasing voltage from –50 to –10 mV, measured at I-V *c* and I-V *d*. Scale bars: 20 ms, 200 pA. **(B)** $Ca_V2.1$ current density as a function of voltage in WT, *Cacna1a*$^{S218L/WT}$, and *Cacna1a*$^{S218L/S218L}$ mice. The $Ca_V2.1$ current was isolated pharmacologically as shown in (A). Peak whole-cell P/Q-type Ba^{2+} currents were divided by the membrane capacitance, normalized to their maximal value and averaged; average normalized *I–V* curves (n = 14, 12, and 10 cells for WT, *Cacna1a*$^{S218L/WT}$, and *Cacna1a*$^{S218L/S218L}$, respectively) were multiplied by the average maximal current densities (n = 35, 44, and 28 cells, respectively). Individual *I–V* curves were fit with the equation $I_{Ba} = G\times(V–E_{rev})/(1+e\text{^}((V_{0.5}–V)/k))$. Average (± SEM) $V_{0.5}$ values were –15 ± 1 (WT), –20.1 ± 0.8 (*Cacna1a*$^{S218L/WT}$; $p < 0.005$ vs. WT) and –25 ± 1 mV (*Cacna1a*$^{S218L/S218L}$; $p < 0.005$ vs. *Cacna1a*$^{S218L/WT}$, $p < 0.00005$ vs. WT). Inset: P/Q-type Ba^{2+} currents elicited at the voltages indicated (pooled from different cells). **(C)** Current densities of L-, N-, and R-type Ca^{2+} channels in WT and *Cacna1a*^{S218L} mice, measured at -10 mV. The different current types were isolated pharmacologically as shown in (A). The current densities for the L-type component were: 10.5 ± 0.7 (n = 24), 12.7 ± 0.7 (n = 27), and 13.8 ± 1.1 (n = 29) pA/pF in *Cacna1a*$^{S218L/S218L}$, *Cacna1a*$^{S218L/WT}$, and WT neurons, respectively; for the N-type: 8.0 ± 0.7 (n = 27), 8.8 ± 0.8 (n = 29), and 6.5 ± 0.8 (n = 29) pA/pF; for the R-type: 23.0 ± 1.6 (n = 28), 20.4 ± 1.0 (n = 43), and 22.9 ± 1.1 (n = 35) pA/pF. The sum of the three components (total non-$Ca_V2.1$ current density) was similar for all three genotypes (41.5 ± 1.9, 41.9 ± 1.5, and 43.2 ± 1.7 pA/pF).

brain water content increased by only 1.51 % in wild-type mice (from 76.99 ± 0.67% to 78.50 ± 1.14%) and by only 1.49% in *Cacna1a*$^{S218L/WT}$ mice (from 77.12 ± 0.94% to 78.61 ± 1.07%). In contrast, in *Cacna1a*$^{S218L/S218L}$ mice, the brain water content increased significantly by 2.84% (from 76.89 ± 0.64% to 79.73 ± 0.93%; $p < 0.02$ *vs.* heterozygous and wild-type mice). Baseline brain water content was similar in all three mice genotypes. Twenty percent of the *Cacna1a*$^{S218L/S218L}$ mice, but none of the wild-type or heterozygous mice, died after these mild impact experiments.

Taken together, these results demonstrate that *Cacna1a*$^{S218L/S218L}$ mice faithfully mimic the broad spectrum of spontaneous episodic, mild impact-triggered, and permanent clinical features seen in S218L patients.

Gain-of-function effect on whole-cell Ca^{2+} influx and synaptic transmission

To understand the molecular consequences of the S218L mutation on $Ca_V2.1$ channel functioning, we performed whole-cell patch-clamp recordings of cerebellar granule neurons (*Fig. 3A*). Neurons expressing S218L channels displayed significantly increased whole-cell $Ca_V2.1$ current density at negative voltages as reflected by a pronounced gene dosage–dependent leftward shift in voltage-dependent activation (*Fig. 3B*). In contrast, current density was not changed at positive voltages, indicating that the number of functional $Ca_V2.1$ channels at the somatodendritic plasma membrane is similar across genotypes (see also *Supplementary note 2*). Moreover, the enhanced Ca^{2+} influx was not accompanied by significant changes in the density of other high voltage–activated Ca_V channels, except for a slight decrease in L-type currents (*Fig. 3C*).

The effects in *Cacna1a*$^{S218L/S218L}$ neurons were reminiscent of the changes seen in neurons of the clinically milder R192Q mice (*van den Maagdenberg et al., 2004*), but were stronger. As a consequence of the even lower activation threshold of S218L channels (*Tottene et al., 2005*), the gain-of-function of the $Ca_V2.1$ current at low voltages was more dramatic in *Cacna1a*$^{S218L/S218L}$ neurons than the gain-of-function we previously observed in *Cacna1a*$^{R192Q/R192Q}$ neurons, leading to Ca^{2+} influx close to the resting potential. While the $Ca_V2.1$ current at -40 mV was approximately 4 times larger in *Cacna1a*$^{R192Q/R192Q}$ neurons compared to wild-type neurons (*van den Maagdenberg et al., 2004*), the $Ca_V2.1$ current in *Cacna1a*$^{S218L/S218L}$ neurons was 6.6 times larger than that in wild-type neurons (*Fig. 3B*).

Consistent with Ca^{2+} influx occurring close to the resting potential, the S218L mutation produced a much larger increase in the frequency of spontaneous transmitter release events (i.e., the MEPPs) at the NMJ when compared with the R192Q mutation. While the MEPP frequency in *Cacna1a*$^{R192Q/R192Q}$ mice was only 2.5 times higher than in wild-type mice (*van den Maagdenberg et al., 2004*), the MEPP frequency in *Cacna1a*$^{S218L/WT}$ was 8.5 times and in *Cacna1a*$^{S218L/S218L}$ 12.5 times higher than in wild-type mice (*Fig. 4A*).

Remarkably, although a similar increase in $Ca_V2.1$ current at -40 mV, relative to their respective wild-type mice, was measured in cerebellar granule neurons from

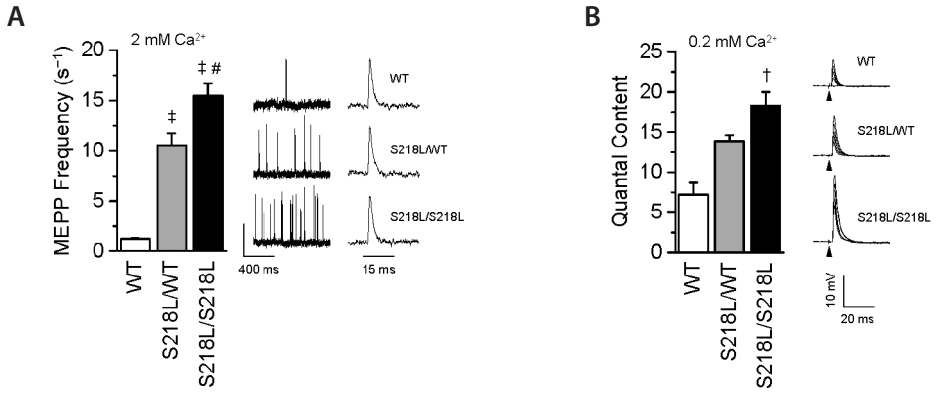

Figure 4. Synaptic transmission at the neuromuscular junction. Synaptic transmission at the NMJ is increased in *Cacna1a*^{S218L} mice. **(A)** Summary of miniature endplate potential (MEPP) frequency (n = 6; ‡, $p < 0.001$ vs. WT; #, $p < 0.01$ vs. *Cacna1a*$^{S218L/WT}$). Exemplar recordings are shown at the right. Vertical scale bar: 0.75 mV. **(B)** Summary of neurotransmitter release in 0.2 mM extracellular Ca^{2+} evoked by supramaximal stimulation of the phrenic nerve (n = 3 mice; †, $p < 0.01$ vs. WT). At the right are exemplar endplate potentials; black triangles mark the stimulation moment.

Cacna1a$^{S218L/WT}$ (2.7 times larger; *Fig. 3B*) and *Cacna1a*$^{R192Q/R192Q}$ (3.8 times larger; *van den Maagdenberg et al., 2004*), the relative increase in MEPP frequency was much greater in *Cacna1a*$^{S218L/WT}$ mice, consistent with higher Ca^{2+} influx at rest in the nerve terminals of these mice. However, quantal content (i.e., the number of neurotransmitter quanta released by an action potential) measured in low extracellular Ca^{2+} was 2.5 times higher in S218L synapses (compared to wild-type; *Fig. 4B*), to a similar extent as in R192Q synapses (3.4 times compared to wild-type; *van den Maagdenberg et al., 2004*). This observation suggests a ceiling effect for release probability at the NMJ.

Extreme susceptibility of S218L mice for CSD

As CSD is the likely underlying mechanism for migraine aura (*Lauritzen, 1994*), and has also been implicated in epilepsy and edema (*Gorji, 2002*), increased susceptibility for CSD in S218L compared to R192Q mice could explain many features of the dramatic S218L syndrome. To test this hypothesis, we assessed the triggering threshold for CSD, the CSD propagation velocity, and the probability of multiple CSD events upon a single stimulus in the two knockin mouse models.

Indeed, *S218L* mice showed both a lower threshold for CSD induction (*Fig. 5A*; for examples of CSD traces, see *Supplementary Fig. 3*) and a faster propagation of CSD waves (*Fig. 5B*) when compared to R192Q mice. In addition, S218L mice had a gene dosage–dependent increased probability of experiencing successive CSD events upon a single stimulus: the probability was the highest in homozygous *Cacna1a*$^{S218L/S218L}$ mice, which carry two copies of the S218L allele, lowest in wild-type mice, and in between in heterozygous

Cacna1a$^{S218L/WT}$ mice, which carry only one copy of the S218L allele (*Fig. 5C*). There was, however, no difference in average latency until the first recurrent CSD between *Cacna1a*$^{S218L/WT}$ (1,323 ± 189 sec) and *Cacna1a*$^{S218L/S218L}$ (1,108 ± 211 sec) (p = 0.35).

It is noteworthy to emphasize that, although CSD induction threshold and propagation velocity are similar in *Cacna1a*$^{S218L/WT}$ and *Cacna1a*$^{R192Q/R192Q}$ mice (*Fig. 5A, B*), multiple CSD events were seen only rarely in *Cacna1a*$^{R192Q/R192Q}$ mice (*Fig. 5C*).

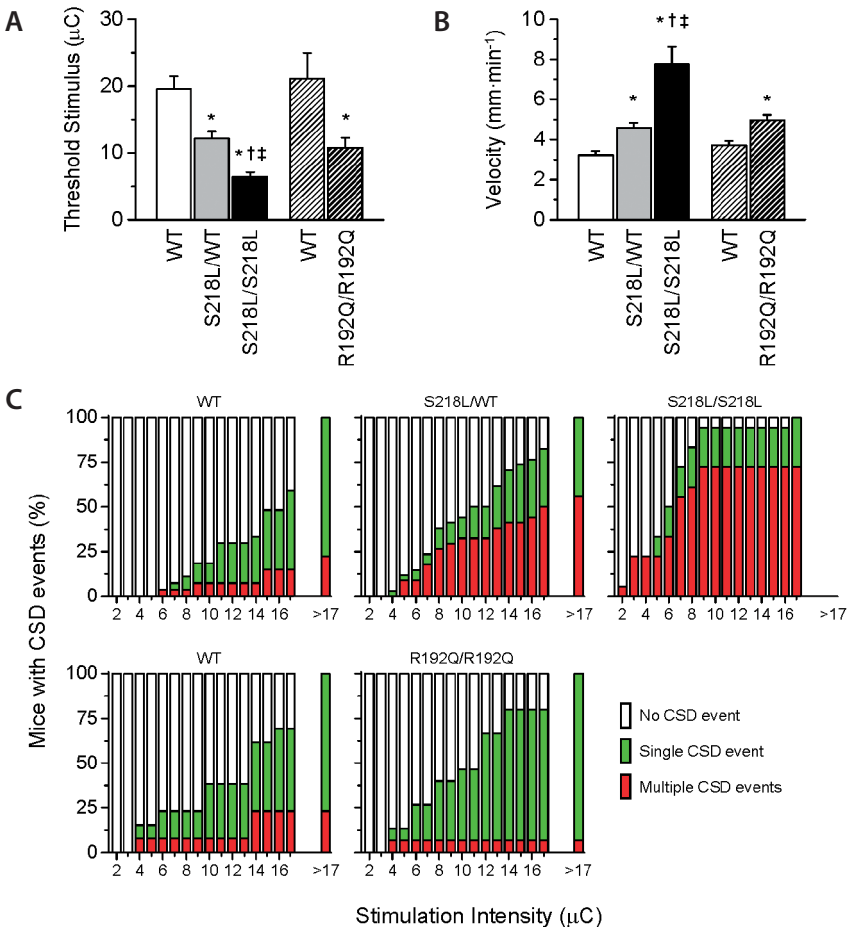

Figure 5. Increased susceptibility to CSD in *Cacna1a*^{S218L} and *Cacna1a*^{R192Q} mice. (A) Summary of the threshold required to elicit at least one CSD event in wild-type, *Cacna1a*^{S218L}, and *Cacna1a*^{R192Q} mice. *Cacna1a*^{S218L} strain: n = 30, 39, and 22 mice for WT, *Cacna1a*$^{S218L/WT}$, and *Cacna1a*$^{S218L/S218L}$, respectively. *Cacna1a*^{R192Q} strain: n = 28 and 31 mice for WT and *Cacna1a*^{R192Q}, respectively. *, $p < 0.05$ vs. WT; †, $p < 0.05$ vs. S218L/WT; ‡, $p < 0.05$ vs. R192Q/R192Q. **(B)** Summary of CSD velocity measured using two recording electrodes (see Methods). Sample sizes are as in (A). *, $p < 0.05$ vs. WT; †, $p < 0.05$ vs. S218L/WT; ‡, $p < 0.05$ vs. R192Q/R192Q. **(C)** Proportion of mice (expressed as a percentage of all mice) with no response, a single CSD or multiple CSD events as a function of stimulation intensity. *Cacna1a*^{S218L} strain: n = 27, 34, and 18 mice for WT, *Cacna1a*$^{S218L/WT}$, and *Cacna1a*$^{S218L/S218L}$, respectively. *Cacna1a*^{R192Q} strain: n = 13 and 15 mice for WT and *Cacna1a*^{R192Q}, respectively.

The selectively high incidence of multiple CSDs in S218L mice makes it unlikely that recurring CSDs would be merely due to tissue damage during CSD recordings. If tissue damage had been the underlying cause, one would have expected a more evenly distributed increased probability of repetitive CSD events over the various genotypes. In contrast, R192Q mice hardly exhibited recurring CSD events. Lastly, great care was taken in monitoring the condition of the cortex. Mice with visible cortical lesions, as identified using a surgical microscope, were excluded from the analyses.

DISCUSSION

Here, we present the generation and behavioral, electrophysiological, and neurobiological characterization of S218L knockin mice bearing the human pathogenic *CACNA1A*^{S218L} missense mutation in $Ca_V2.1$ calcium channels. In humans this mutation causes a broad and devastating, sometimes even fatal, clinical syndrome, with both episodic and progressive features of brain dysfunction. In this respect, the S218L syndrome is at the very end of the clinical spectrum of migraine. Our findings can be summarized as follows:

1) S218L mice display a complex phenotype consisting of: (1) mild permanent cerebellar ataxia; (2) spontaneous attacks of hemiparesis and/or (sometimes fatal) seizures; and (3) brain edema following only a very mild head impact. These features faithfully mimic the clinical spectrum of patients carrying the *CACNA1A*^{S218L} mutation (*Fitzsimons et al., 1985*; *Kors et al., 2001*; *Curtain et al., 2006*; *Chan et al., 2008*).

2) Most of the functional consequences of the S218L FHM1 mutation are qualitatively similar to, but quantitatively far more pronounced than those of the R192Q FHM1 mutation; this correlates well with the milder phenotype that is seen in patients with the R192Q mutation and strongly supports the view that these changes are causally relevant. Specifically, when compared to *Cacna1a*$^{R192Q/R192Q}$ neurons (*van den Maagdenberg et al., 2004*; *Kaja et al., 2005*; *Tottene et al., 2009*; *this study*), *Cacna1a*$^{S218L/S218L}$ neurons have: (1) a greater increase in $Ca_V2.1$-mediated Ca^{2+} current density upon weak depolarization; (2) a larger increase in spontaneous neurotransmitter release at the NMJ, a model synapse in the peripheral nervous system that relies exclusively on $Ca_V2.1$ channels and can be electrophysiologically analyzed with relative ease; and (3) a greater susceptibility for CSD, as reflected by a lower triggering threshold, higher propagation velocity, and a higher probability of successive CSD events upon only a single stimulus (see also below). Moreover, heterozygous *Cacna1a*$^{S218L/WT}$ and homozygous *Cacna1a*$^{R192Q/R192Q}$ mice showed quantitatively similar gain-of-function effects in Ca^{2+} current density and CSD threshold and velocity. However, spontaneous neurotransmitter release at the NMJ was much larger in *Cacna1a*$^{S218L/WT}$ mice, suggesting a larger Ca^{2+} influx at rest in nerve terminals. In contrast with the good correlation between severity of the phenotype and facilitation of both neuronal Ca^{2+} current and CSD, the facilitation of evoked release at the NMJ at low extracellular Ca^{2+} was similar in *Cacna1a*$^{S218L/S218L}$ and

Cacna1a$^{R192Q/R192Q}$ mice. In fact, at physiological extracellular [Ca^{2+}] evoked release at the NMJ of both mutant mice (*data not shown*) was not different from that at wild-type NMJs. *Tottene et al.* (2009) reported an enhanced evoked glutamate release at excitatory cortical pyramidal cell synapses of *Cacna1a*$^{R192Q/R192Q}$ mice at physiological [Ca^{2+}], but an unaltered evoked GABA release from inhibitory fast-spiking (FS) interneuron synapses (despite being also controlled by $Ca_V2.1$ channels). Thus, the NMJ may perhaps be a better model for cortical inhibitory FS interneuron synapses than cortical excitatory synapses, whose gain-of-function was shown to be causally linked to CSD facilitation (*Tottene et al., 2009*).

3) The S218L FHM1 mutation, but not the R192Q FHM1 mutation, increased the probability of multiple CSD events in response to only a *single* threshold stimulus. While wild-type and R192Q mice generally experienced a single CSD event upon a single stimulus, S218L mice showed a gene dosage-dependent increased probability of having successive CSD events. This tendency of S218L mice for successive CSD events is particularly remarkable given that, despite similar CSD induction threshold and propagation velocity for *Cacna1a*$^{R192Q/R192Q}$ and *Cacna1a*$^{S218L/WT}$ mice (*Fig. 5A, B*), multiple CSD events are seen only rarely in *Cacna1a*$^{R192Q/R192Q}$ mice (*Fig. 5C*). Thus, the cortical susceptibility to repetitive CSD events is apparently unique to the S218L mutation.

The exact mechanism for recurrent CSD events following a single stimulus and the exact downstream consequences of multiple CSD events remain to be determined. The combination of the more negative activation threshold of S218L $Ca_v2.1$ channels coupled with both their impaired inactivation during depolarization and faster recovery from inactivation (*Tottene et al., 2005*), suggests the involvement of a process that is particularly sensitive to Ca^{2+} influx at rest, channel inactivation, or both. Perhaps, prolonged Ca^{2+} influx during the first CSD event may be involved as well.

Our findings suggest that the high sensitivity of the S218L brain to even mild stimuli (e.g., low-impact head trauma) may be explained, at least in part, by the unique combination of a particularly low CSD trigger threshold and a high propensity for multiple CSD events. Increased susceptibility to the effects of successive CSD events may also play a role. By analogy, we propose that similar mechanisms underlie the severe and clinically broad phenotype that is seen in S218L patients, but not in patients carrying other, milder FHM1 mutations. Thus, our data provide a mechanistic basis for the *overlapping* clinical manifestations of both R192Q and S218L patients as well as for the *additional* severe clinical features seen only in S218L patients.

There is ample evidence that migraine, mild head trauma-triggered migraine attacks (such as in footballer's migraine), brain edema, epilepsy, and (subclinical) cerebellar ataxia can co-occur in various combinations (*Blau & Solomon, 1985*; *Solomon, 1998*; *Sándor et al., 2001*; *Gorji et al., 2001*; *Stam et al., 2008*; *Ambrosini et al., 2008*; *Rogawski, 2008*; *Haan et al., 2008*). This suggests shared molecular disease pathways. For instance, both migraine attacks and seizures are associated with excessive neuronal excitability

in the cortex (*Rogawski, 2008*). While CSD is well recognized as the pathophysiological correlate of the migraine aura (*Hadjikhani et al., 2001*; *Bowyer et al., 2001*), its role in epilepsy is less clear. Clearly, there is a distinction between spreading depression and hypersynchronous activity in seizures, but it appears that spreading depression may gradually evolve into "spreading convulsions" when waves occur at high frequency (*Whieldon & van Harreveld, 1950*). *Eikermann-Haerter et al.* (*2009*) recently showed that generalized seizures may occur 45-75 min after a single KCl-induced CSD in homozygous *Cacna1a*^{S218L} mice, but not in *Cacna1a*^{R192Q} mice, indicating that CSD and epileptic events are separated in time. Follow-up studies, comparing the exact conditions under which CSD and epilepsy may occur in $Ca_v2.1$ mutant mouse types, are likely to shed further light on the similarities and dissimilarities of these two apparently opposing neuronal mechanisms underlying episodic brain dysfunction.

CSD has also been implicated in edema (*Gorji et al., 2001*). In rodents, waves of spreading depression caused transient severe neuronal swelling, changes in dendritic structures (*Takano et al., 2007*), and prolonged severe vascular leakage with impairment of the blood-brain barrier (*Gursoy-Ozdemir et al., 2004*). Opening of the blood-brain barrier, which possibly is secondary to multiple CSD events, preceded cortical edema in a patient with a severe attack of FHM type 2 caused by an *ATP1A2* mutation (*Dreier et al., 2005*). We, therefore, like to speculate that the unique vulnerability of the S218L brain to multiple CSD events may underlie the dramatic and sometimes fatal clinical features in both S218L patients and mice. Future experiments are needed to address the issue of whether the edema is a direct consequence of trauma, or is due to either trauma-induced CSD or epilepsy.

As yet, it is unclear how the S218L mutation may cause cerebellar ataxia. One can speculate that the ataxia may be due to excessive Ca^{2+} influx in cerebellar Purkinje cells, to a differential effect of the mutation on the afferent inputs of Purkinje cells, or both. These mechanisms are likely to disturb the delicately-regulated firing patterns of the Purkinje cells, as suggested earlier by studies in naturally-occurring *Cacna1a* mouse mutants (*Hoebeek et al., 2005*; *Walter et al., 2006*).

Despite the advantages that our R192Q and S218L mice seem to have to study disease mechanisms, it is also clear that the model needs further validation. For instance, it needs to be established whether R192Q and S218L mice can experience migraine attacks and whether transgenic mice are indeed useful models to study migraine. Although, the S218L mice seem helpful in investigating how a single $Ca_V2.1$ mutation may lead to a combination of clinical phenotypes (i.e., hemiplegic migraine, seizures, cerebellar ataxia, and mild head trauma-induced edema) seen in FHM1 S218L patients, it is also clear that the co-occurrence of phenotypes in these mice makes it much harder to study the effect of a $Ca_V2.1$ mutation on *specific* phenotypes. In this respect, it is uncertain whether these mice will advance our knowledge on understanding disease mechanisms of, for instance, hemiplegic migraine or cerebellar ataxia. A direct extrapolation of results from mice to patients should be done with great caution, as there are obvious

differences in the physiology between humans and experimental animal models. Future studies will have to show the benefits and limitations of these transgenic mouse models.

In summary, we report here that S218L FHM1 mice faithfully seem to mimic the salient clinical features of the broad human S218L hemiplegic migraine syndrome, and we propose a mechanistic explanation for these severe clinical features. Despite the limitations mentioned above, we believe that the S218L and R192Q knockin FHM1 mouse models will likely serve as valuable tools in unraveling, at least to some extent, the mechanisms of FHM, common migraine, epilepsy, and cerebral edema.

ACKNOWLEDGEMENTS

We thank M.L. Maat-Schieman, S. van Duijnen, S. Verbeek (LUMC, Leiden, The Netherlands) for help in histological experiments and ES injections, and E. Hess (Johns Hopkins University School of Medicine, Baltimore) for expert opinions on the evaluation of the behavioral phenotype. In addition, we thank E. Putignano, U. Nehrdich, and R. van der Giessen for technical assistance. This work was supported by grants of the Netherlands Organization for Scientific Research (NWO) (903-52-291, to M.D.F, R.R.F., and Vici 918.56.602, to M.D.F), the EU "EUROHEAD" grant (LSHM-CT-2004-504837) (to D.P. and M.D.F) and the Center of Medical System Biology (CMSB) established by the Netherlands Genomics Initiative/Netherlands Organisation for Scientific Research (NGI / NWO) and Community (to M.D.F., R.R.F. and A.M.J.M. v.d. M); Telethon Italy, Italian Ministry of Education University Research (PRIN, FIRB) (to D.P.); the Prinses Beatrix Fonds (MAR01-0105), the Hersenstichting Nederland (9F01(2).24), and KNAW van Leersumfonds (to J.J.P.); the Dutch ZON-MW Organization for Medical Sciences, ALW Life Sciences, Senter (Neuro-Bsik), Prinses Beatrix Fonds, and the SENSOPAC program of the European Community (to C.d.Z.). S.K. was European Molecular Biology Organization postdoctoral fellow and trainee of the Michael Smith Foundation for Health Research.

SUPPLEMENTARY MATERIAL

Supplementary notes

1. EEG recordings of epileptic attacks in homozygous Cacna1a^{S218L} mice

Long-term EEG recordings and parallel video observation were performed in three *Cacna1a*$^{S218L/S218L}$, three *Cacna1a*$^{S218L/WT}$, and one wild-type mouse. Only the three *Cacna1a*$^{S218L/S218L}$ mice exhibited attacks. Details on the individual phases, duration, and frequency of attacks are described below. All three *Cacna1a*$^{S218L/S218L}$ mice suffered from epileptic attacks that notably had the same sequence of phases, although there was considerable variation in the duration of these phases (see *Fig. 2D* for an example series of EEG traces of a typical epileptic attack that was lethal). All attacks started with the mouse jumping in the cage with an upright tail during which the EEG shows spike discharges; this phase lasted 10-15 min and likely represents myoclonic jerks (*trace 2*). Then the mouse fell on one side and exhibited vigorous trains of simultaneous contraction of all extremities, during which the EEG shows negative polyspike discharges (*trace 3*). Based on these characteristics, we considered these to be clonic seizures. These attacks developed into clonic-tonic seizures as clonic seizures were interrupted by brief (~10 s) episodes of contractions during which all extremities were extended and appear stiff. During the clonic-tonic phase, the EEG showed positive and/or negative polyspike discharges (*traces 4* and *5*). This phase lasted around 30 min, and was followed by reduced EEG activity, after which the mouse became active and ran in circles (5-15 min). Occasionally, the mouse would stumble due to brief abrupt muscle contractions. At this stage, the outcome varied among attacks. Either the mouse fell on one side, had a few contractions, and died (*trace 6*), or it has a flat EEG for 2

min and survived. Initially, surviving mice had shallow breathing with no response to painful stimuli. After about 10 min, they could right themselves but were largely immobile for 20 min with normal EEG patterns. Following this phase, the mice exhibited normal behaviour until had another attack (see below). Of the three *Cacna1a*$^{S218L/S218L}$ mice, one had a lethal attack after 4 h into the EEG recording session. The second mouse survived its first attack (after 7 h of EEG recording) and had a second, lethal, attack 11h later. The third mouse survived two attacks (after 8 and 25 h into the EEG recording session) before it died during the third attack at 48 h.

2. Quantification of density of functional $Ca_V2.1$ channels by electrophysiology.
Electrophysiological experiments of $Ca_V2.1$ channels in granule cells (*Fig. 3B*) allowed the quantification of the density of *functional* $Ca_V2.1$ channels at the plasma membrane. At voltages above of 0 mV, where $Ca_V2.1$ channels have maximal open probability ($P_{o,max}$), the whole-cell $Ca_V2.1$ current density (I_{Ba}) in *Cacna1a*$^{S218L/S218L}$ and *Cacna1a*$^{S218L/WT}$ neurons was similar to that in wild-type neurons. Because S218L-mutated and wild-type $Ca_V2.1$ channels have similar $P_{o,max}$ and identical single channel current (*Tottene et al., 2005*), *i*, this implies a similar density of functional $Ca_V2.1$ channels (*N*) at the plasma membrane for all three genotypes (given that $I = N \cdot i \cdot P_o$) (*Tottene et al., 2002*). Similar results were obtained when studying granule cell neurons of R192Q-mutated and wild-type $Ca_V2.1$ channels (*van den Maagdenberg et al., 2004*). Thus, the estimated density of functional $Ca_V2.1$ channels is not affected by either the S218L or R192Q mutation, and the increased current density at negative voltages can be fully explained by a negative shift in the voltage dependence of activation.

Supplementary methods

Histology and immunohistochemistry
For the analysis of gross cytoarchitecture, the animals were sacrificied by intracardial perfusion with 4% PFA and processed for standard histochemical staining with hematoxylin and eosin (H&E) and Klüver-Barrera. For Golgi-Cox staining of Purkinje cells, 2 months old animals were intracardially perfused with PBS. Brains were immediately removed from the cranium and Golgi-Cox staining was performed as described earlier (*Glaser & van der Loos, 1981*). Golgi-Cox–stained sections were used to assess the dendritic arborization of Purkinje cells using the linear Sholl analysis (*Sholl, 1953*; *Espinosa et al., 2009)*. In short, concentric circles increasing in size (with 15 µm intervals) were aligned with the Purkinje cell soma. The number of Purkinje cell dendrites intersecting with the circle were counted. Data from Purkinje cells were analyzed per genotype. For the same cells, we also measured the distance from the Purkinje cell soma to the first dendrite branching point (the primary Purkinje cell dendritic length).

For immunohistochemistry, brains of adult mice (~3 months old) were obtained after perfusion with PBS followed by 4% PFA fixation. Post-fixation was done for 1-2hrs in 4% PFA followed by overnight incubation in 10% sucrose/0.1 M phosphate buffer at 4ºC. Subsequently, membranes were removed, tissue was embedded in 10% sucrose/11% gelatine, and gelatin was fixed with 30% sucrose/10% formaline for 2.5 h at room temperature, followed by overnight incubation in 30% sucrose/0.1 M phosphate buffer at 4ºC. After freezing down, coronal sections of 40 µm were processed free-floating during whole procedure. For immunohistochemistry, antigen retrieval was performed for 30 min at 80ºC in 10 mM citrate buffer (pH 5.5). Sections were incubated in 10% heat-inactivated FCS/0.5%TX100/TBS for 2hrs and then incubated with primary $Ca_v2.1$-α_1 antibody (*Chemicon, Temecula, CA*) 1:200 diluted in 2% heat-inactivated FCS/0.4%TX100/TBS at 4ºC. Secondary biotin-labeled goat anti-rabbit antibody (*Vector Laboratories, Burlingame, CA*) (1:200 diluted in the same buffer) incubation was performed for 2hrs at room temperature. Finally, for detection, sections were incubated with the avidin-biotin kit (*Vector Laboratories*) for 2hrs at room temperature, washed, and developed in 0.1 mg/ml diaminobenzidine with 0.005% H_2O_2. In control experiments, immunoreactivity of the $Ca_V2.1$-α_1 antibody could be blocked after adding the peptide against which the antibody was generated. Specificity of the $Ca_V2.1$-α_1 antibody was previously shown by *Kulik et al.* (*2004*).

Supplementary references

1. Espinosa JS, Wheeler DG, Tsien RW, Luo L. Uncoupling dendrite growth and patterning: single-cell knockout analysis of NMDA receptor 2B. Neuron. 2009;62:205-17.
2. Glaser EM, van der Loos H. Analysis of thick brain sections by obverse-reverse computer microscopy: application of a new, high clarity Golgi-Nissl stain. J Neurosci Methods. 1981;4:117-25.
3. Kulik A, Nakadate K, Hagiwara A, Fukazawa Y, Luján R, Saito H, Suzuki N, Futatsugi A, Mikoshiba K, Frotscher M, Shigemoto R. Immunocytochemical localization of the alpha 1A subunit of the P/Q-type calcium channel in the rat cerebellum. Eur J Neurosci. 2004;19:2169-78.
4. Sholl DA. Dendritic organization in the neurons of the visual and motor cortices of the cat. J Anat. 1953;87:387-406.
5. Tottene A, Fellin T, Pagnutti S, Luvisetto S, Striessnig J, Fletcher C, Pietrobon D. Familial hemiplegic migraine mutations increase Ca^{2+} influx through single human CaV2.1 channels and decrease maximal $Ca_V2.1$ current density in neurons. Proc Natl Acad Sci USA. 2002;99:13284-9.
6. Tottene A, Pivotto F, Fellin T, Cesetti T, van den Maagdenberg AM, Pietrobon D. Specific kinetic alterations of human CaV2.1 calcium channels produced by mutation S218L causing familial hemiplegic migraine and delayed cerebral edema and coma after minor head trauma. J Biol Chem. 2005;280:17678-86.
7. van den Maagdenberg AM, Pietrobon D, Pizzorusso T, Kaja S, Broos LA, Cesetti T, van de Ven RC, Tottene A, van der Kaa J, Plomp JJ, Frants RR, Ferrari MD. A *Cacna1a* knockin migraine mouse model with increased susceptibility to cortical spreading depression. Neuron. 2004;41:701-10.

Supplementary figures

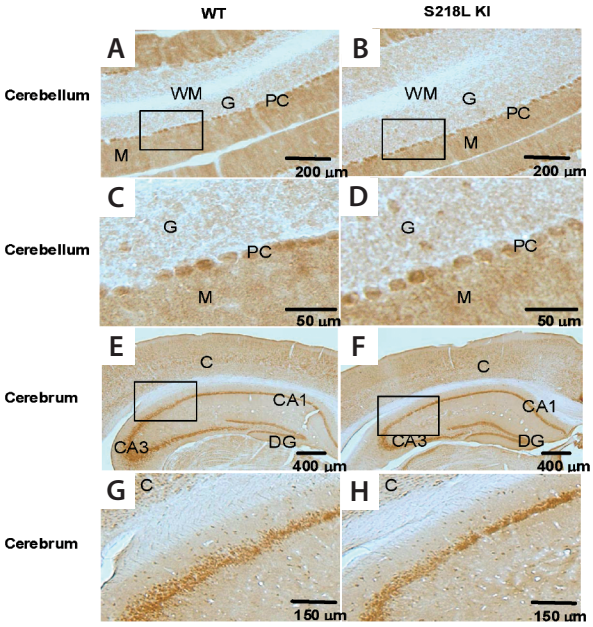

Supplementary Figure 1. $Ca_v2.1$-α_1 staining in brains of *Cacna1a*$^{S218L/S218L}$ mice. Expression of $Ca_v2.1$-α_1 protein with immunostaining in brains of wild-type (WT) (left column) and *Cacna1a*$^{S218L/S218L}$ (right column) mice. Expression patterns of $Ca_v2.1$-α_1 protein in coronal sections of cerebellum **(A-D)** and cerebrum **(E-H)** are comparable between WT and *Cacna1a*$^{S218L/S218L}$ mice. Boxes in panels A, B, E, and F are presented at higher magnification in panels C, D, G and H, respectively. C - cerebral cortex; DG - dentate gyrus; WM - white matter; G - granule cell layer; M - molecular layer PC - Purkinje cell layer.

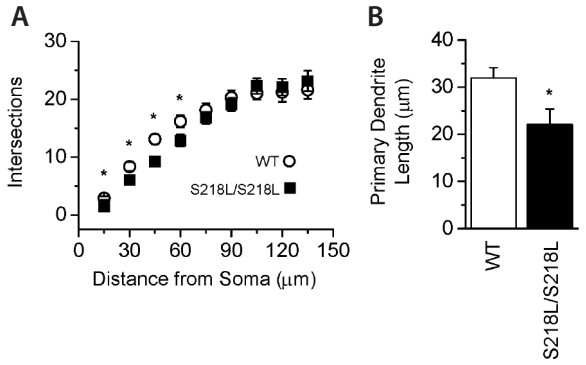

Supplementary Figure 2. A quantification of the dendritic arborisation of Purkinje cells was performed on Golgi-Cox–stained sections using the linear Sholl analysis. (A) Concentric circles were aligned on the soma of a Purkinje cell with increasing diameter and the number of intersections of dendrites with the circles was counted. Arborization of dendrites close to the soma is less dense in the *Cacna1a*$^{S218L/S218L}$ mice. Open and closed circles indicate data from wild-type (WT) and *Cacna1a*$^{S218L/S218L}$ mice (S218L/S218L), respectively. In total, 30 (WT) and 24 (S218L/S218L) Purkinje cells from 3 WT and 3 S218L/S218L mice were analyzed per genotype. To avoid a possible bias due to unbalanced numbers of cells analyzed per animal, ≥ 7 Purkinje cells were analyzed per animal. Asterisks indicate that for the four most proximal circles, *Cacna1a*$^{S218L/S218L}$ mice showed significantly less intersections than wild-type mice ($p < 0.05$ using Student's *t*-tests for the individual data points). A repeated-measures ANOVA test[7] that included all 9 data points did not show a significant difference ($p = 0.36$) between *Cacna1a*$^{S218L/S218L}$ and wild-type mice. **(B)** Quantification of the length of primary dendrites of the same Purkinje cells was measured as the distance between the edge of the soma and the first branching point of the proximal dendrite. The asterisk indicates a statistically significant difference (Student's *t*-test: $p < 0.005$). Values represent mean ± S.E.M.

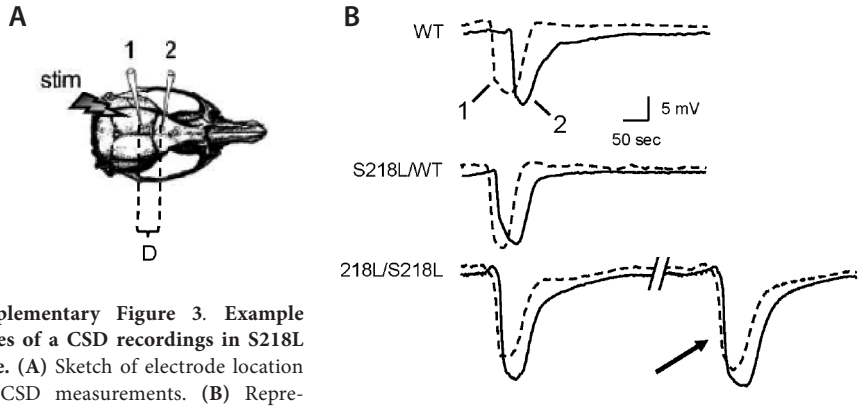

Supplementary Figure 3. Example traces of a CSD recordings in S218L mice. (A) Sketch of electrode location for CSD measurements. **(B)** Representative CSD traces in wild-type (WT), *Cacna1a*$^{S218L/WT}$, and *Cacna1a*$^{S218L/S218L}$ mice. The arrow indicates a recurrent CSD in a *Cacna1a*$^{S218L/S218L}$ mouse after a single stimulus. The dotted and normal lines represent traces of the first and second electrode, respectively. The gap in the trace of the S218L/S218L mouse is 350 s. Stim - stimulus electrode. D - distance between the two recording electrodes.

REFERENCES

1. Adams PJ, Snutch TP. Calcium channelopathies: voltage-gated calcium channels. Subcell Biochem. 2007;45:215-51.
2. Barrett CF, Cao YQ, Tsien RW. Gating deficiency in a familial hemiplegic migraine type 1 mutant P/Q-type calcium channel. J Biol Chem. 2005;280:24064-71.
3. Blau JN, Solomon F. Migraine and intracranial swelling: an experiment of nature. Lancet. 1985;28:718.
4. Bolay H, Reuter U, Dunn AK, Huang Z, Boas DA, Moskowitz MA. Intrinsic brain activity triggers trigeminal meningeal afferents in a migraine model. Nat Med. 2002;8:136-42.
5. Bowyer SM, Aurora KS, Moran JE, Tepley N, Welch KM. Magnetoencephalographic fields from patients with spontaneous and induced migraine aura. Ann Neurol. 2001;50:582-7.
6. brosini A, Sándor PS, De Pasqua V, Pierelli F, Schoenen J. Performances in cerebellar and neuromuscular transmission tests are correlated in migraine with aura. J Headache Pain. 2008;9:29-32.
7. Cao YQ, Piedras-Rentería ES, Smith GB, Chen G, Harata NC, Tsien RW. Presynaptic Ca^{2+} channels compete for channel type-preferring slots in altered neurotransmission arising from Ca^{2+} channelopathy. Neuron. 2004;43:387-400.
8. Cao YQ, Tsien RW. Effects of familial hemiplegic migraine type 1 mutations on neuronal P/Q-type Ca2+ channel activity and inhibitory synaptic transmission. Proc Natl Acad Sci USA. 2005;102:2590-5.
9. Catterall WA. Structure and function of neuronal Ca2+ channels and their role in neurotransmitter release. Cell Calcium. 1998;24:307-23.
10. Cha YH, Millett D, Kane M, Jen J, Baloh R. Adult-onset hemiplegic migraine with cortical enhancement and oedema. Cephalalgia. 2007;27:1166-70.
11. Chan YC, Burgunder JM, Wilder-Smith E, Chew SE, Lam-Mok-Sing KM, Sharma V, Ong BK. Electroencephalographic changes and seizures in familial hemiplegic migraine patients with the CACNA1A gene S218L mutation. J Clin Neurosci. 2008;15:891-4.
12. Chen Y, Constantini S, Trembovler V, Weinstock M, Shohami E. An experimental model of closed head injury in mice: pathophysiology, histopathology, and cognitive deficits. J Neurotrauma. 1996;13:557-68.
13. Curtain RP, Smith RL, Ovcaric M, Griffiths LR. Minor head trauma-induced sporadic hemiplegic migraine coma. Pediatr Neurol. 2006;34:329-32.
14. Dreier JP, Jurkat-Rott K, Petzold GC, Tomkins O, Klingebiel R, Kopp UA, Lehmann-Horn F, Friedman A, Dichgans M. Opening of the blood-brain barrier preceding cortical edema in a severe attack of FHM type II. Neurology. 2005;64:2145-7.
15. Ducros A, Denier C, Joutel A, Cecillon M, Le-

scoat C, Vahedi K, Darcel F, Vicaut E, Bousser MG, Tournier-Lasserve E. The clinical spectrum of familial hemiplegic migraine associated with mutations in a neuronal calcium channel. New Engl J Med. 2001;345:17-24.

16. Eikermann-Haerter K, Dileköz E, Kudo C, Savitz SI, Waeber C, Baum MJ, Ferrari MD, van den Maagdenberg AM, Moskowitz MA, Ayata C. Genetic and hormonal factors modulate spreading depression and transient hemiparesis in mouse models of familial hemiplegic migraine type 1. J Clin Invest. 2009;119:99-109.
17. Ferrari MD, Goadsby PJ. Migraine as a cerebral ionopathy with abnormal central sensory processing. In Neurobiology of Disease, eds Gilman S, Pedley T: Elsevier, New York, 2006; 333-48.
18. Ferrari MD. Migraine. Lancet. 1998;351:1043-51.
19. Fitzsimons RB, Wolfenden WH. Migraine coma. Meningitic migraine with cerebral oedema associated with a new form of autosomal dominant cerebellar ataxia. Brain. 1985;108:555-77.
20. Fletcher CF, Tottene A, Lennon VA, Wilson SM, Dubel SJ, Paylor R, Hosford DA, Tessarollo L, McEnery MW, Pietrobon D, Copeland NG, Jenkins NA. Dystonia and cerebellar atrophy in CACNA1A null mice lacking P/Q calcium channel activity. FASEB J. 2001;15:1288-90.
21. Gorji A. Spreading depression: a review of the clinical relevance. Brain Res Brain Res Rev. 2001;38:33-60.
22. Gursoy-Ozdemir Y, Qiu J, Matsuoka N, Bolay H, Bermpohl D, Jin H, Wang X, Rosenberg GA, Lo EH, Moskowitz MA. Cortical spreading depression activates and upregulates MMP-9. J Clin Invest. 2004;113:1447-55.
23. Haan J, Kors EE, Vanmolkot KR, van den Maagdenberg AM, Frants RR, Ferrari MD. Migraine genetics: an update. Curr Pain Headache Rep. 2005;9:213-20.
24. Haan J, Terwindt GM, van den Maagdenberg AM, Stam AH, Ferrari MD. A review of the genetic relation between migraine and epilepsy. Cephalalgia. 2008;28:105-13.
25. Hadjikhani N, Sanchez Del Rio M, Wu O, Schwartz D, Bakker D, Fischl B, Kwong KK, Cutrer FM, Rosen BR, Tootell RB, Sorensen AG, Moskowitz MA. Mechanisms of migraine aura revealed by functional MRI in human visual cortex. Proc Natl Acad Sci USA. 2001;98:4687-92.
26. Hans M, Luvisetto S, Williams ME, Spagnolo M, Urrutia A, Tottene A, Brust PF, Johnson EC, Harpold MM, Stauderman KA, Pietrobon D. Functional consequences of mutations in the human alpha(1A) calcium channel subunit linked to familial hemiplegic migraine. J Neurosci. 1999;19:1610-9.
27. Headache Classification Subcommittee of the International Headache Society. The international classification of headache disorders: 2nd edition. Cephalalgia. 2004;24:1-160.
28. Hoebeek FE, Stahl JS, van Alphen AM, Schonewille M, Luo C, Rutteman M, van den Maagdenberg AM, Molenaar PC, Goossens HH, Frens MA, De Zeeuw CI. Increased noise level of Purkinje cell activities minimizes impact of their modulation during sensorimotor control. Neuron. 2005;45:953-65.
29. Kaja S, van de Ven RC, Broos LA, Frants RR, Ferrari MD, van den Maagdenberg AM, Plomp JJ. Characterization of acetylcholine release and the compensatory contribution of non-Ca(v)2.1 channels at motor nerve terminals of leaner Ca(v)2.1-mutant mice. Neuroscience. 2007;144:1278-87.
30. Kaja S, van de Ven RC, Broos LA, Veldman H, van Dijk JG, Verschuuren JJ, Frants RR, Ferrari MD, van den Maagdenberg AM, Plomp JJ. Gene dosage-dependent transmitter release changes at neuromuscular synapses of CACNA1A R192Q knockin mice are non-progressive and do not lead to morphological changes or muscle weakness. Neuroscience. 2005;135:81-95.
31. Kaplan EL, Meier P. Nonparametric Estimation from Incomplete Observations. J Am Stat Ass. 1958;53:457-81.
32. Kors EE, Terwindt GM, Vermeulen FL, Fitzsimons RB, Jardine PE, Heywood P, Love S, van den Maagdenberg AM, Haan J, Frants RR, Ferrari MD. Delayed cerebral edema and fatal coma after minor head trauma: role of CACNA1A calcium channel subunit gene and relationship with familial hemiplegic migraine. Ann Neurol. 2001;49:753-60.
33. Kraus RL, Sinnegger MJ, Glossmann H, Hering S, Striessnig J. Familial hemiplegic migraine mutations change alpha(1A) Ca^{2+} channel kinetics. J Biol Chem. 1998;273:5586-90.
34. Kraus RL, Sinnegger MJ, Koschak A, Glossmann H, Stenirri S, Carrera P, Striessnig J. Three new familial hemiplegic migraine mutants affect P/Q-type Ca(2+) channel kinetics. J Biol Chem. 2000;275:9239-43.
35. Lakso M, Pichel JG, Gorman JR, Sauer B, Okamoto Y, Lee E, Alt FW, Westphal H. Efficient in vivo manipulation of mouse genomic sequences at the zygote stage. Proc Natl Acad Sci USA.

1996;93:5860-5.

36. Lauritzen M. Pathophysiology of the migraine aura. The spreading depression theory. Brain. 1994;117:199-210.
37. lter JT, Alviña K, Womack MD, Chevez C, Khodakhah K. Decreases in the precision of Purkinje cell have making cause cerebellar dysfunction and ataxia. Nat Neurosci. 2006;9:389-97.
38. Magleby KL, Stevens CF. The effect of voltage on the time course of end-plate currents. Physiol. 1972;223:151-71.
39. McLachlan EM, Martin AR. Non-linear summation of end-plate potentials in the frog and mouse. J Physiol. 1981;311:307-24.
40. Meaney JF, Williams CE, Humphrey PR. Case report: transient unilateral cerebral oedema in hemiplegic migraine: MR imaging and angiography. Clin Radiol. 1996;51:72-6.
41. Ophoff RA, Terwindt GM, Vergouwe MN, van Eijk R, Oefner PJ, Hoffman SM, Lamerdin JE, Mohrenweiser HW, Bulman DE, Ferrari M, Haan J, Lindhout D, van Ommen GJ, Hofker MH, Ferrari MD, Frants RR. Familial hemiplegic migraine and episodic ataxia type-2 are caused by mutations in the Ca^{2+} channel gene CACNL1A4. Cell. 1996;87:543-52.
42. Pietrobon D. Familial hemiplegic migraine. Neurotherapeutics. 2007;4:274-84.
43. Rogawski MA. Common pathophysiologic mechanisms in migraine and epilepsy. Arch Neurol. 2008;65:709-14.
44. Sándor PS, Mascia A, Seidel L, de Pasqua V, Schoenen J. Subclinical cerebellar impairment in the common types of migraine: a three-dimensional analysis of reaching movements. Ann Neurol. 2001;49:668-72.
45. Solomon S. John Graham Senior Clinicians Award Lecture. Posttraumatic migraine. Headache. 1998;38:772-8.
46. Stam AH, van den Maagdenberg AM, Haan J, Terwindt GM, Ferrari MD. Genetics of migraine: an update with special attention to genetic comorbidity. Curr Opin Neurol. 2008;21:288-93.
47. Takano T, Tian GF, Peng W, Lou N, Lovatt D, Hansen AJ, Kasischke KA, Nedergaard M. Cortical spreading depression causes and coincides with tissue hypoxia. Nat Neurosci. 2007;10:754-62.
48. Terwindt GM, Ophoff RA, Haan J, Vergouwe MN, van Eijk R, Frants RR, Ferrari MD. Variable clinical expression of mutations in the P/Q-type calcium channel gene in familial hemiplegic migraine. Neurology. 1998;50:1105-10.
49. Tottene A, Conti R, Fabbro A, Vecchia D, Shapovalova M, Santello M, van den Maagdenberg AM, Ferrari MD, Pietrobon D. Enhanced excitatory transmission at cortical synapses as the basis for facilitated spreading depression in Ca(v)2.1 knockin migraine mice. Neuron. 2009;61:762-73.
50. Tottene A, Fellin T, Pagnutti S, Luvisetto S, Striessnig J, Fletcher C, Pietrobon D. Familial hemiplegic migraine mutations increase Ca2+ influx through single human CaV2.1 channels and decrease maximal CaV2.1 current density in neurons. Proc Natl Acad Sci USA. 2002;99:13284-9.
51. Tottene A, Pivotto F, Fellin T, Cesetti T, van den Maagdenberg AM, Pietrobon D. Specific kinetic alterations of human CaV2.1 calcium channels produced by mutation S218L causing familial hemiplegic migraine and delayed cerebral edema and coma after minor head trauma. J Biol Chem. 2005;280:17678-86.
52. Uchitel OD, Protti DA, Sanchez V, Cherksey BD, Sugimori M, Llinás R. P-type voltage-dependent calcium channel mediates presynaptic calcium influx and transmitter release in mammalian synapses. Proc Natl Acad Sci USA. 1992;89:3330-3.
53. Vakili A, Kataoka H, Plesnila N. Role of arginine vasopressin V1 and V2 receptors for brain damage after transient focal cerebral ischemia. J Cereb Blood Flow Metab. 2005;25:1012-9.
54. Van den Maagdenberg AM, Haan J, Terwindt GM, Ferrari MD. Migraine: gene mutations and functional consequences. Curr Opin Neurol. 2007;20:299-305.
55. van den Maagdenberg AM, Pietrobon D, Pizzorusso T, Kaja S, Broos LA, Cesetti T, van de Ven RC, Tottene A, van der Kaa J, Plomp JJ, Frants RR, Ferrari MD. A Cacna1a knockin migraine mouse model with increased susceptibility to cortical spreading depression. Neuron. 2004;41:701-10.
56. Whieldon JA, van Harreveld A. Cumulative effects of minimal cortical stimulation. EEG Clin Neurophysiol. 1950;179:49-57.
57. Zweckberger K, Erös C, Zimmermann R, Kim SW, Engel D, Plesnila N. Effect of early and delayed decompressive craniectomy on secondary brain damage after controlled cortical impact in mice. J Neurotrauma. 2006;23:1083-93.
58. Zwingman TA, Neumann PE, Noebels JL, Herrup K. Rocker is a new variant of the voltage-dependent calcium channel gene Cacna1a. J Neurosci. 2001;21:1169-78.